Acta Biomaterialia 101 (2020) 314–326

Contents lists available at ScienceDirect

Acta Biomaterialia

journal homepage: www.elsevier.com/locate/actbio

Full length article

Porous chitosan adhesives with L-DOPA for enhanced photochemical tissue bonding

Herleen Ruprai[a], Anu Shanu[b], Damia Mawad[c,d], James M. Hook[e,f], Kristopher Kilian[c,f], Laurel George[g], Richard Wuhrer[g], Jessica Houang[h], Simon Myers[a,b], Antonio Lauto[a,b,i,*]

[a] School of Science and Health, Western Sydney University, Locked Bag 1797, Penrith, NSW 2751, Australia
[b] School of Medicine, Western Sydney University, Locked Bag 1797, Penrith, NSW 2751, Australia
[c] School of Materials Science and Engineering, University of New South Wales, Sydney, NSW 2052, Australia
[d] Australian Centre for NanoMedicine, ARC Centre of Excellence in Convergent BioNano Science and Technology, and Centre for Advanced Macromolecular Design, University of New South Wales, Sydney, NSW 2052, Australia
[e] Mark Wainwright Analytical Centre, University of New South Wales, Sydney, NSW 2052, Australia
[f] School of Chemistry, University of New South Wales, Sydney, NSW 2052, Australia
[g] Advanced Materials Characterization Facility, Western Sydney University, Locked Bag 1797, Penrith, NSW 2751, Australia
[h] Biomedical Engineering, School of Aerospace, Mechanical and Mechatronic Engineering, University of Sydney, Sydney, NSW 2006, Australia
[i] Biomedical Engineering and Neuroscience Research Group, The MARCS Institute, Western Sydney University, Locked Bag 1797, Penrith, NSW 2751, Australia

ARTICLE INFO

Article history:
Received 22 May 2019
Revised 27 September 2019
Accepted 30 October 2019
Available online 2 November 2019

Keywords:
Biomaterials
Adhesive films
Tissue repair
Sutureless
Photoactive

ABSTRACT

L-3,4-dihydroxyphenylalanine (L-DOPA) is a naturally occurring catechol that is known to increase the adhesive strength of various materials used for tissue repair. With the aim of fortifying a porous and erodible chitosan-based adhesive film, L-DOPA was incorporated in its fabrication for stronger photochemical tissue bonding (PTB), a repair technique that uses light and a photosensitiser to promote tissue adhesion. The results showed that L-DOPA did indeed increase the tissue bonding strength of the films when photoactivated by a green LED, with a maximum strength recorded of approximately 30 kPa, 1.4 times higher than in its absence. The addition of L-DOPA also did not appreciably change the swelling, mechanical and erodible properties of the film. This study showed that strong, porous and erodible adhesive films for PTB made from biocompatible materials can be obtained through a simple inclusion of a natural additive such as L-DOPA, which was simply mixed with chitosan without any chemical modifications. *In vitro* studies using human fibroblasts showed no negative effect on cell proliferation indicating that these films are biocompatible. The films are convenient for various surgical applications as they can provide strong tissue support and a microporous environment for cellular infusion without the use of sutures.

Statement of significance

Tissue adhesives are not as strong as sutures on wounds under stress. Our group has previously demonstrated that strong sutureless tissue repair can be realised with chitosan-based adhesive films that photochemically bond to tissue when irradiated with green light. The advantage of this technique is that films are easier to handle than glues and sutures, and their crosslinking reactions can be controlled with light. However, these films are not optimal for high-tension tissue regenerative applications because of their non-porous structure, which cannot facilitate cell and nutrient exchange at the wound site. The present study resolves this issue, as we obtained a strong and porous photoactivated chitosan-based adhesive film, by simply using freeze drying and adding L-DOPA.

* Corresponding author at: School of Science and Health, Western Sydney University, Locked Bag 1797, Penrith, NSW 2751, Australia.
E-mail addresses: 17995131@student.westernsydney.edu.au (H. Ruprai), a.shanu@westernsydney.edu.au (A. Shanu), damia.mawad@unsw.edu.au (D. Mawad), j.hook@unsw.edu.au (J.M. Hook), k.kilian@unsw.edu.au (K. Kilian), l.george@westernsydney.edu.au (L. George), richard.wuhrer@westernsydney.edu.au (R. Wuhrer), jhou5747@uni.sydney.edu.au (J. Houang), s.myers@westernsydney.edu.au (S. Myers), a.lauto@westernsydney.edu.au (A. Lauto).

https://doi.org/10.1016/j.actbio.2019.10.046
1742-7061/

1. Introduction

Tissue adhesives have shown considerable potential as an alternative to sutures in a number of surgical procedures, particularly in those requiring a tight seal to prevent fluid leakage [1]. Adhesives are advantageous over sutures in that they are faster to apply, less painful and less invasive [1]. However, their high cost and confined scope of applicability due to biocompatibility concerns, slow degradation or weak approximation of wound edges under wet or high-tension conditions, limits their widespread clinical acceptance [1]. Alternative methods to sutures are sought out because these techniques are challenging to use on small anatomical structures such as nerves and impede the healing process by causing foreign body reactions or tissue distortions at the surgical site [2].

A promising adhesive that we have developed to overcome the aforementioned issues, is the biocompatible and green light-activated rose bengal-chitosan adhesive for photochemical tissue bonding (PTB). PTB is a repair technique that promotes collagen crosslinking using light and a photosensitiser with minimal heat production [2–4]. The fabrication of this adhesive is simple and scalable: no chemical modification is required to produce an insoluble and free-standing chitosan film. It is biocompatible as demonstrated by implantation around the nerves for 3 months [2], and its degradation profiles can be controlled by adding lysozymes in the films [5]. Of note, this adhesive has a high bonding strength ($\sim$ 21 kPa) when structured with nanopillars [6]. The nanopillars increase tissue bonding by mimicking the van der Waal interactions afforded by nano-scaled setae on the toes of the gecko. However, strong adhesion can only be achieved when the film is non-porous, which reduces the film's ability to allow for cell and nutrient exchange required for healing.

In this study, we have fabricated an adhesive film for PTB, with a structure that is both porous and erodible, and with improved adhesion capabilities, achieved through three simple modifications: (1) the film was made porous through freeze drying since freeze-dried chitosan scaffolds have shown to provide a favourable microporous environment for tissue regeneration [7]; (2) oligomeric chitosan (water-soluble chitosan) was introduced to increase erosion rate of the film for better tissue integration, because films previously based solely on medium weight (MW) chitosan were slow to degrade, (less than 10% of the film) after one month *in vivo* [5]. In a previous study, we showed that chitosan films become more soluble with oligomeric chitosan [8]. The addition of oligomeric chitosan is also more cost effective than incorporating enzymes or using multi-step chemical procedures. (3) L-3,4-dihydroxyphenylalanine (L-DOPA) was added to the formulation since previous studies have shown that chemically grafting and blending L-DOPA or catechol groups with chitosan, significantly increased tissue bonding strength [9–15]. In this study, L-DOPA was mixed with chitosan to avoid chemical modification and a possible complex manufacturing process. We hypothesized that rose bengal and green light would not only mediate photochemical tissue bonding [16,17], but also further bonding via oxidation of L-DOPA. This is possible because oxidised catechol groups covalently bond with amine, imidazole and thiol residues that are found in tissue proteins [18].

Green light photosensitisers have been reported to initiate the photooxidation and promote crosslinking of catechol modified hydrogels [19]. This feature is important because light can act as a trigger to control when and where tissue bonding takes place. This is unlike for many catechol-based tissue adhesives in literature, which are often less user friendly because they incorporate a liquid crosslinker or oxidising agent that must be premixed with the adhesive material on the tissue surface. To analyse the effect of these three modifications, we characterised the film's adhesive, swelling, mechanical and erosion properties and biocompatibility with human fibroblast cells.

2. Materials and methods

2.1. Materials

Oligomeric chitosan (MW < 5 kDa; 85% deacetylated, see Fig. S1) was obtained from AK Biotech (Jinan, China). All other chemicals including medium MW chitosan (MW = 190 – 310 kDa; 78% deacetylated, see Fig. S2) and were purchased from Sigma-Aldrich (Sydney, Australia) and used without modification. Cell culture media and supplements for *in vitro* studies were purchased from GIBCO Invitrogen. Cell culture dishes were purchased from Greiner, USA (Interpath). Human fibroblasts (MRC-5 cells, ATCC) were a kind gift from the Stenzel laboratory in the School of Chemistry at UNSW. Small intestine tissue sections (20 cm) were immediately harvested from euthanised sheep (Wollondilly Abattoir Pty Ltd.), cleaned with water and stored at – 80 °C. Prior to experimental use, the tissue sections were thawed and flushed with water at room temperature ($\sim$ 25 °C) and the mesenteric tissue was removed.

2.2. Adhesive film preparation

The solutions were made by following the protocol detailed by Lauto and colleagues [20]. Briefly, chitosan, rose bengal and acetic acid were stirred in deionised water at room temperature ($\sim$ 25 °C) for 2 weeks. To avoid photobleaching of rose bengal, the solutions were shielded with aluminium foil. The solutions were then centrifuged for 1 h, at 3270 x g, at 25 °C and the decanted supernatants were stored at 4 °C until further use. L-DOPA was added to the solution (pH $\sim$ 4) with rose bengal, oligomeric chitosan and MW chitosan, and mixed for 24 h to ensure complete dissolution. A 1:10 molar ratio of L-DOPA to chitosan glucosamine units was present in the solution. Oligomeric chitosan was incorporated in the formulation to make the adhesives films erode faster [8]. The composition of the solutions used for fabricating the adhesive films are shown in Table 1.

The adhesive chitosan films were made from the prepared solutions by pipetting into plastic Petri dishes ($3 \times 4\,cm^2$), 3 mL for porous films and 2.3 mL for non-porous films. Solvent evaporation was then carried out either by air drying under dark cover (room temperature $\sim$ 25 °C for 3 weeks, for non-porous films) or freeze drying (pre-frozen at – 30 °C for 24 h and freeze dried at – 50 °C, 0.1 mbar for 6 h, for porous films). The porous films were also further air dried at room temperature under dark cover for 3 weeks to reduce their water content. The dried films were cut to the desired dimensions for the experimental tests and stored at room temperature between clean glass slides and wrapped with parafilm and aluminium foil. The thickness of the flattened porous and non-porous films when gauged at five different points with a digital micrometer model (293–831, Mitutoyo, Japan) ranged between 340 – 370 µm and 20 – 25 µm, respectively.

2.3. Green light irradiation

The films were layered with tissue and irradiated with green light for $\sim$ 6 min to enable their photochemical bonding to the tissue. The irradiation parameters used are summarised in Table 2 and the light was delivered through an optical fibre (core diameter 200 µm) coupled to a light-emitting diode (LED) system (Ultra High-Power Microscope LED, Prizmatix, USA). The effect of the green light on the erosion, swelling, mechanical properties, L-DOPA oxidation and biocompatibility for the L-DOPA films was also assessed and compared to films without L-DOPA. For these tests, to

Table 1
Solutions composition for adhesive films.*

Solution	Medium MW Chitosan (% w/v)	Oligomeric Chitosan (% w/v)	Acetic Acid (% v/v)	Rose Bengal (% w/v)	L-DOPA (% w/v)
Standard	1.70	0	2	0.01	0
OC	1.53	0.17	2	0.01	0
OC+DOPA	1.53	0.17	2	0.01	0.16

* The label 'Standard' represents the standard composition used in previous studies [3,20]; 'OC' indicates the composition with oligomeric chitosan; 'OC+DOPA' indicates the composition with oligomeric chitosan and L-DOPA. Components were dissolved in deionised water.

Table 2
Irradiation parameters for PTB.*

Peak Wavelength (nm)	Spot Diameter (cm)	Power (mW)	Irradiance ($W\,cm^{-2}$)	Fluence ($J\,cm^{-2}$)
515	~ 0.5	~ 180	~ 0.9	~ 110

* The films were spot-irradiated (~ 5 s per spot) with a continuous wave of green light delivered through an optical fibre coupled to a LED system.

mimic physiological conditions, the films were immersed in phosphate buffer saline (PBS) for ~ 5 s before being exposed to the green light.

2.4. Tissue adhesion measurements

The tissue bonding strength of the films was tested on similar *in vitro* models described by Frost and coworkers [21]. The procedure involved irradiating the film either above ("on top") or below ("on bottom") the serosa of sheep small intestine tissue. Sheep small intestine was chosen because it is large enough to provide tissue for several tests. The serosa is also rich in collagen, which is found in many tissues.

2.4.1. Adhesive "on top"

Strips of tissue measuring $1.5 \times 4\,cm^2$ were cut and bisected. To photochemically reconnect the bisected tissue, the pieces were approximated end-to-end under an operating microscope (20x magnification) and a film ($0.6 \times 1.0\,cm^2$) was placed over the bisection line on the serosa layer, which was irradiated as outlined in Section 2.3. The repaired sample was then clamped into a single column calibrated tensiometer (3384, Instron, USA) and subjected to a loading rate of $22\,mm\,min^{-1}$ until sample fracture was achieved. The bonding strength was estimated by dividing the maximum force measured on the tensiometer force *vs* distance profile by the area of the film. The tissue adhesion energy was calculated by measuring the area under the tensiometer force *vs* distance profile using the tensiometer software (Instron, BlueHill 2). The tissue was kept moist during the repair and before tensile testing to avoid desiccation and to mimic *in vivo* conditions. Tissue repaired with films without LED irradiation were also tested for comparison. To examine whether the release time of L-DOPA affected the bonding strength, selected films were left on the tissue for 0, 3, 6 or 9 before irradiation. Selected films with 10 times less L-DOPA were also tested to find out whether L-DOPA concentration influences the bonding strength (these films were fabricated as outlined in Section 2.2 but L-DOPA was added at 0.016% w/v).

2.4.2. Adhesive "on bottom"

The semi-transparent serosa layer of the intestinal tissue was firstly isolated by gently scraping off the muscularis, submucosa and mucosa layers with a spatula. The serosa was then cut into smaller strips, bisected and reconnected as described in Section 2.4.1, however the sample was inverted such that the green light penetrated the serosa layer first. This enabled the irradiation to reach the film-tissue interface without being heavily attenuated by the film. The bonding strength and tissue adhesion energy of the film was estimated as described in Section 2.4.1. The serosa was also kept moist during the repair and before tensile testing to avoid desiccation and to mimic *in vivo* conditions.

2.5. Atomic force spectroscopy

To investigate the adhesive properties of the films at the nanoscale, the surface of the films was characterised with the atomic force microscope (AFM) (NanoWizard II, JPK Instruments, Germany). Silicon cantilevers tips (SICON, AppNano, USA; spring constant $0.3\,N\,m^{-1}$; resonant frequency 14 – 17 kHz) were used to probe the film surface and were individually calibrated with the thermal noise method before use. The force spectroscopy measurements were performed in deionised water to minimise capillary effects and the following parameters were held constant: Z-length = 2.0 µm, extend time = 2.0 s and relative setpoint = 5 nN. AFM force *vs* extension profiles were obtained at nine different locations over a $50 \times 50\,\mu m^2$ sample area for six films from each group (n = 54). The energy required to detach the AFM tip from the sample surface was calculated as the area under the AFM force *vs* extension curve using the JPK Data Processing software and was recorded as the AFM tip adhesion energy.

2.6. Erosion behaviour

The erosion behaviour of the film was tested *in vitro* by immersing the films in PBS at 37 °C for 7 days and measuring their percentage mass loss at different time points. Briefly, films of size $2 \times 2\,cm^2$ were initially weighed (m_i) and then immersed in 50 mL of PBS 37 °C for 7 days, with daily transfer into fresh PBS. At day 1, 3, 5 and 7, the films were taken out, lyophilised and reweighed (m_d). The mass loss was calculated by comparing the initial dry mass of the film to its dry mass after immersion in PBS for a certain time period, as shown in Eq. (1).

$$\%\ \text{mass loss} = \frac{m_i - m_d}{m_i} \times 100 \quad (1)$$

2.7. Swelling study

The film's swelling properties were tested *in vitro* by suspending pre-weighed films (m_i) of size $2 \times 2\ cm^2$ in PBS at 37 °C. The films were removed at different time points, gently dry-blotted with a Kim Wipe and reweighed (m_s). The swelling ratio of a film at each time point was then calculated using Eq. (2):

$$\%\ \text{swelling ratio} = \frac{m_s - m_i}{m_i} \times 100 \quad (2)$$

2.8. Mechanical properties

The tensile properties of the films were measured with a 3343 Instron tensiometer. Films of size $0.6 \times 3.0\,cm^2$ were clamped in the tensiometer and subjected to a tensile loading rate of $22\,mm\,min^{-1}$ until cohesive failure occurred (i.e. the film broke into two pieces). Prior to the tensile test, the films were hydrated in PBS for ~ 10 s to mimic the wet conditions *in vivo*. The force

vs distance profiles were converted to stress-strain curves and the Young's modulus was calculated as the tangent slope at the linear portion on these graphs using the tensiometer software (Instron, Bluehill 2). The maximum tensile stress (tensile strength) and maximum tensile strain (percentage elongation) was also recorded (film thickness and width were assumed constant during the test).

2.9. Scanning electron microscopy

Images of the surface of the porous films and the tissue – adhesive interface were obtained using a JEOL 6510 low vacuum scanning electron microscope (SEM). The porous films were prepared for examination by leaving them unflattened after fabrication for better pore visibility, then cutting them to $0.5 \times 0.5\,cm^2$ squares, which were attached to aluminium stubs with double sided conductive carbon tape. A low vacuum pressure of 30 Pa in the SEM allowed samples to be examined uncoated. Images were taken with a backscatter detector, an accelerating voltage of 15 kV, and a working distance of roughly 12 mm.

To verify whether the addition of L-DOPA affected the pore size, SEM images collected at a magnification of 50x were used to measure and compare the pore diameters for both the OC+DOPA and the OC porous films. A total of 300 pores from each group were measured (6 films from each group; 50 pores per film) using the Aperio ImageScope program. The pore diameter was defined as the square root of the shortest and longest diameter of the pore since the pores were not perfectly circular. To observe the adhesive-tissue interface, transverse sections ($0.5 \times 0.3\,cm^2$) of the photochemically bonded adhesive and intestinal tissue were cut and immediately fixed in Karnovsky's solution (2% v/v glutaraldehyde and 2.5% w/v paraformaldehyde in 0.1 M PBS) at 4 °C. After 24 h, the samples were rinsed with PBS for 15 min and dehydrated with a graded series of ethanol with concentrations of 30, 50 and 70% v/v. The dried samples were then fixed onto to aluminium stubs with double sided conductive carbon tape and run under the same conditions as mentioned above.

2.10. Spectroscopic observation of L-DOPA oxidation

Irradiation induced L-DOPA oxidation was qualitatively studied using ultraviolet-visible (UV–Vis) spectroscopy to record the wavelength of absorption peaks. More detailed analysis, such as measuring the concentration of oxidized products, is problematic as L-DOPA produces various intermediate products upon oxidation. Furthermore, the opacity of the L-DOPA porous films made spectrophotometric readings impossible, thus the films (with and without irradiation) were dissolved in 5 mL of 2%v/v acetic acid in deionised water. The absorbance spectra of 1 mL aliquots in quartz cuvettes were then recorded at wavelengths from 200 to 700 nm at room temperature (~ 25 °C) using a Shimadzu UV-1800 UV–Vis spectrophotometer. All samples were initially referenced against 2% v/v acetic acid blanks in deionised water before recording their spectra.

2.11. L-DOPA release study

The rate of L-DOPA release for the porous and non-porous films was compared by measuring the amount of L-DOPA released from a film ($0.6 \times 1.0\ cm^2$) when immersed in 5 mL of PBS at room temperature (~ 25 °C). The films were left for 6 min in PBS as this corresponded to how long the films were on tissue when photochemically bonded at room temperature. Afterwards, 1 mL of the PBS was collected and placed in a quartz cuvette. The absorbance of the aliquot was measured at 280 nm and converted to a mass value using a calibration curve of known L-DOPA concentrations in PBS following which the ratio of the average mass of L-DOPA released between non-porous and porous films was calculated. This ratio was compared to the mass ratio of L-DOPA within the non-porous and porous films. A mass ratio was used because these films have different amounts of L-DOPA (the non-porous film contains ~ $307\,\mu g/cm^2$ and the porous films contains ~ $400\,\mu g/cm^2$). The films have different amounts of L-DOPA because the porous films were made from a larger volume of the adhesive solution (Section 2.2).

The percentage of L-DOPA released from the films over time was also measured for films that produced the highest bonding strength. These films ($0.6 \times 1.0\,cm^2$) were placed in 5 mL of PBS at room temperature (~ 25 °C) and taken out of the PBS at different time intervals. The mass of L-DOPA released in the PBS was quantified in the same way as described above. The percentage release of L-DOPA was then calculated at each time point (the mass of L-DOPA released in the PBS was divided by the mass of L-DOPA in a 0.6 cm^2 film and then multiplied by 100) and plotted as a function of release time.

2.12. Biocompatibility study

Human fibroblasts (MRC-5 cells) were seeded on selected films with and without irradiation to quantitatively and qualitatively assess the film's biocompatibility. Films without rose bengal were also tested. These films were fabricated as described in Section 2.2 but the solutions were mixed for 1 week instead of 2 weeks; chitosan mixtures with rose bengal require longer stirring due to rose bengal's poor solubility in acidic conditions. The films ($0.5 \times 0.5\,cm^2$) were sterilised with 70% ethanol, washed with PBS and placed in a 12-well culture plate before adding the cells. The cells were seeded at 10^5 cells/well and grown for 6 days with the films and 5 mL of DMEM media containing 10% foetal bovine serum (FBS; Bovogen), 100 U/mL penicillin, 100 µg/mL streptomycin, 2 mM L-glutamine and 1% (v/v) non-essential amino acid solution at 37 °C in a humidified atmosphere containing 5% CO_2. Cells plated in the wells with media and without the films were used as controls.

2.12.1. Cell viability assay

Cell viability was measured based on the reduction of methylthiazolyldiphenyl-tetrazolium bromide (MTT), to purple formazan crystals by metabolically active cells. Cells were gently washed with warm PBS and incubated with 0.5 mg/mL MTT compound dissolved in Hank's balanced salt solution (HBSS) at 37 °C for 4 h. Cells incubated without films were used as controls and cells treated with 6% ethanol were used as negative controls. Following incubation, HBSS was removed from wells and the purple formazan crystals were dissolved in 1 mL of dimethyl sulfoxide, and 200 µL aliquots were transferred into 96 well plates, in duplicates and absorbance was measured at 570 nm. Cell viability was quantitatively measured by calculating cell viability as fold change of mean absorbance values against control cells.

2.12.2. Live/Dead cell imaging

In order to qualitatively assess the viability of cells growing on the film, cells were stained with Calcein-AM and propidium-iodide (PI), based on the principle that Calcein-AM stains the live cells green and (PI) stains the dead cell nuclei red. Briefly, cells seeded on the films were washed with warm PBS and incubated at 37 °C with HBSS containing 5 µM Calcein-AM for 30 min. Following incubation, cells were washed and loaded with HBSS containing PI (5 µM) and fluorescence was imaged using an inverted Olympus IX51 microscope at 4X magnification. Cells incubated without films were used as positive controls and cells treated with 6% ethanol were used as negative controls.

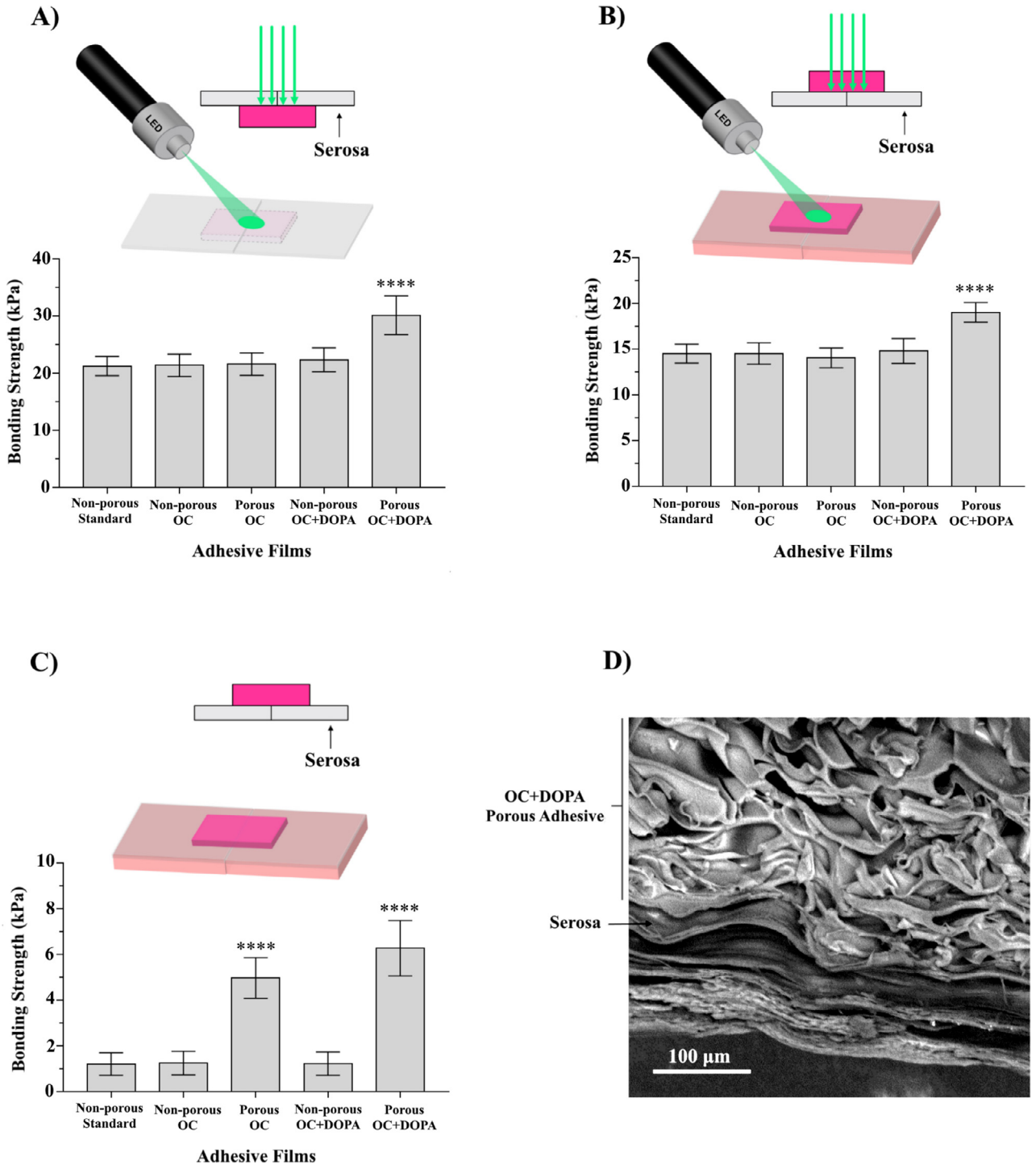

Fig. 1. Bonding strength of irradiated adhesive films placed on bottom (A) and top (B) of the sheep small intestine serosa. C) shows the bonding strength of the same groups on top of the serosa without green light exposure. The porous OC+DOPA films resulted in the highest bonding strength in all tests. All films failed predominantly (> 60%) at the tissue interface except for the porous OC+DOPA films tested in A), which failed cohesively in all trials. Data represent mean ± standard deviation ($n = 30$) and p values determined by one-way ANOVA, Tukey's post-test where **** represents $p < 0.0001$. D) shows a cross-sectional SEM image of the porous OC+DOPA film photochemically bonded to sheep small intestinal tissue. The serosa conforms closely with the pore profile of the adhesive. (For interpretation of the references to color in this figure legend, the reader is referred to the web version of this article.)

2.13. Statistics

Unpaired two-tailed t-tests or analysis of variance (ANOVA) one-way with Tukey's post-tests were used to analyse the data. Means were considered significantly different if $p < 0.05$. Values are expressed as mean ± standard deviation and 'n' represents the number of samples tested for a group.

3. Results and discussion

3.1. Tissue bonding strength

When the films were placed on the bottom of the serosa tissue layer and irradiated (Section 2.4.2), the porous OC+DOPA films achieved a bonding strength of 30 ± 3 kPa ($n = 30$). This was

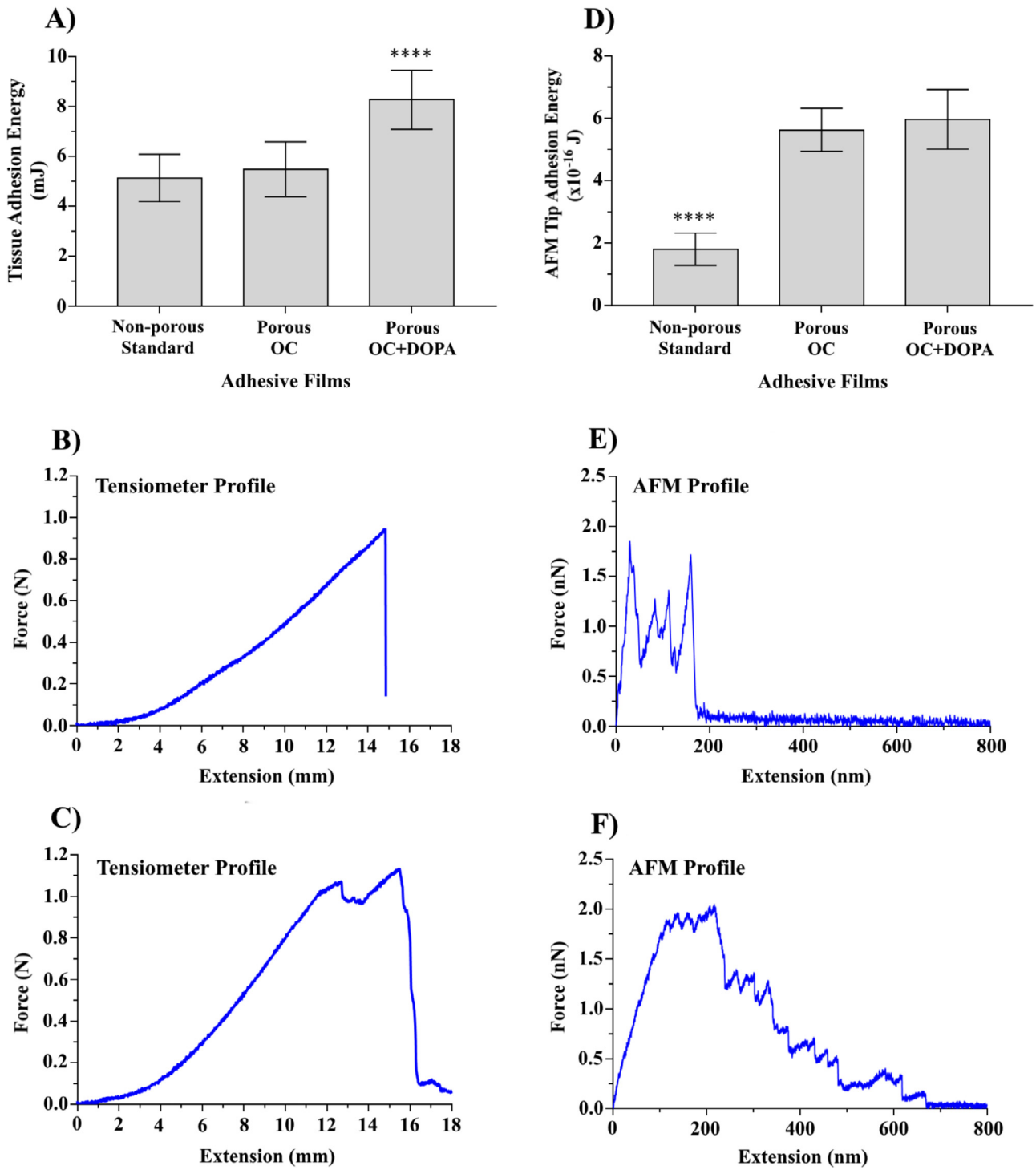

Fig. 2. Adhesion energy of adhesive films when measured with the tensiometer and AFM. Plot A) shows the tissue adhesion energy of non-porous standard, porous OC and porous OC+DOPA films when photochemically bonded on top of sheep small intestine tissue; the porous OC+DOPA films were the toughest to detach from the tissue. Typical tensiometer force *vs* extension curves of tissue repaired with the non-porous standard film and the porous OC+DOPA film are depicted in B) and C) respectively. Plot D) shows the energy required to detach an AFM silicon tip for the same three groups; the toughness of the porous OC and porous OC+DOPA films were similar but both greater than the non-porous standard films. Typical AFM force *vs* extension curves are depicted for the non-porous standard film and the porous OC+DOPA film in E) and F) respectively. In these profiles, when the AFM tip moves up and away from the surface of the film, the tethered chitosan polymer chains electrostatically attracted to the tip are 'stretched' and consequently rupture, resulting in the multiple peaks shown in the graphs. Data is displayed as mean ± standard deviation where $n = 30$ for A) and $n = 54$ for D). P values were determined by one-way ANOVA, Tukey's post-test, where **** signifies $p < 0.0001$.

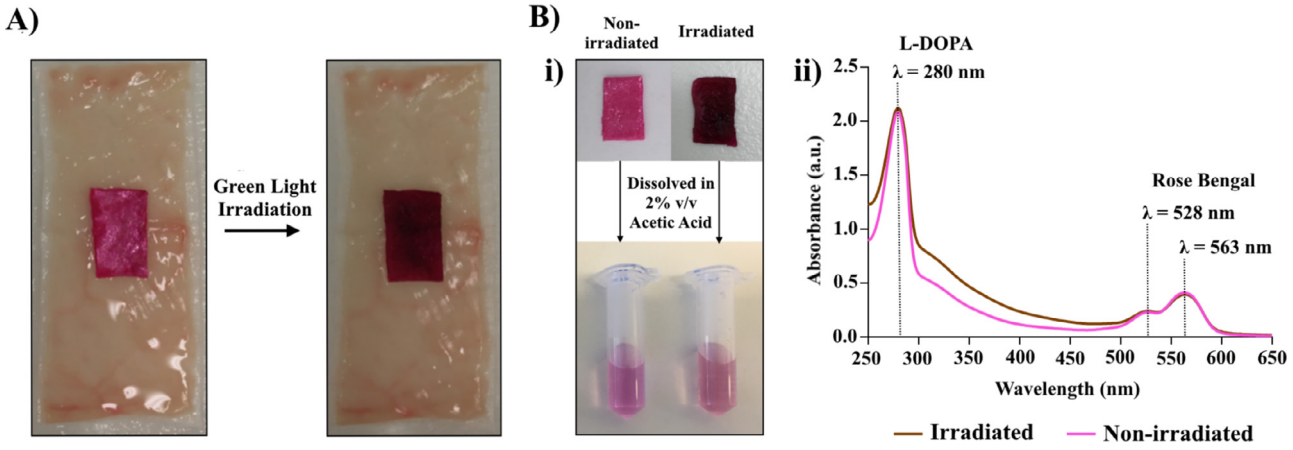

Fig. 3. Visual and spectroscopic observation of L-DOPA oxidation within the porous OC+DOPA films when irradiated with green light. A) depicts the browning of the porous OC+DOPA films when photochemically bonded to sheep small intestine tissue (film size ~ $1.0 \times 0.6\,cm^2$); left image displays the film before LED irradiation and the right image shows the film after ~ 6 min of LED irradiation. The browning of the adhesive is characteristic of products from L-DOPA oxidation [9,29,32]. Bi) depicts typical porous OC+DOPA films with and without irradiation that were dissolved in 2% v/v aqueous acetic acid to record their spectra. Bii) shows representative UV–Vis spectra of 1 mL aliquots from the dissolved samples shown in Bi). When the films were irradiated, the absorbance in the 300–500 nm range increased, indicating the formation of products with catecholquinones [12,28]. (For interpretation of the references to color in this figure legend, the reader is referred to the web version of this article.)

significantly higher than all other adhesives tested, which had bonding strengths within 19 – 25 kPa ($p < 0.0001$, one-way ANOVA, Tukey's post-test) (Fig. 1A). Tissue separation in the repairs using OC+DOPA porous adhesives was due to cohesive failure; all other films failed predominately (> 60%) at the tissue interface. When the films were on top of the serosa tissue layer and irradiated (Section 2.4.1), the bonding strength of the porous OC+DOPA films (19 ± 1 kPa, $n = 30$) was still significantly higher than all the adhesives tested in this study (13 – 16 kPa) ($p < 0.0001$, one-way ANOVA, Tukey's post-test) (Fig. 1B). Tissue separation during these repairs was mostly (> 70%) at the tissue interface for all films. The bonding strength of the films placed above the serosa is expected to be lower since light is attenuated more readily by the films due to their greater thickness. Without green light exposure, all films had much lower bonding strengths (Fig. 1C), as photochemical crosslinking reactions did not occur. Interestingly, the OC+DOPA porous films also had significantly higher bonding strengths (6 ± 1 kPa, $n = 30$) than all groups in this test (1 – 5 kPa) ($p < 0.0001$, one-way ANOVA, Tukey's post-test). It also seems that porosity may enhance tissue bonding via mechanical interlocking (Fig. 1D), as the porous films had higher bonding strengths than the non-porous films (Fig. 1C). All films in these repairs failed at the tissue interface.

Catechols have been used to increase the tissue bonding of many tissue adhesives [22,23]. Studies have shown improved tissue bonding when catechols are incorporated with chitosan. For example, a catechol and chitosan hydrogel treated with $NaIO_4$ produced an adhesive strength on rabbit intestine that was ~ 2 times stronger than a chitosan hydrogel alone [9]. A catechol conjugated chitosan porous patch was also able to produce ~ 4 times higher bonding strength on mouse subcutaneous tissue than the porous patch with just chitosan [10]. In this study, to simplify the fabrication procedure, L-DOPA was not chemically attached to chitosan. Our L-DOPA modified rose bengal-chitosan porous films, when photoactivated, were ~ 1.4 times stronger than the non-porous rose bengal-chitosan (standard) films used in previous studies; *in vivo*, these non-porous films can withstand the stresses of a beating heart [24], and provide similar repair strengths to sutures when used for nerve repair [4,25]. The high bonding strength of the OC+DOPA porous films may be useful for clinical procedures that required enhanced support to stabilize the wound such as tendon repairs [26].

3.2. Adhesion energy

The adhesion properties of the porous OC+DOPA films were further characterized to establish whether their bonding energy was also superior. Using the tensiometer, the tissue adhesion energy of the porous OC+DOPA films (8 ± 1 mJ) was found to be significantly higher ($p < 0.0001$, one-way ANOVA, Tukey's post-test, $n = 30$) than the non-porous standard films (5 ± 1 mJ) and the porous OC films (5 ± 1 mJ), when placed on top of the tissue and irradiated (Fig. 2A). When AFM tip adhesion energy was measured, the non-porous standard films had significantly lower values (Fig. 2D), indicating; the porous films have a higher adhesion toughness. The AFM tip adhesion energy for the non-porous standard, porous OC+DOPA and porous OC films were $(2 \pm 1) \times 10^{-16}$ J, $(6 \pm 1) \times 10^{-16}$ J and $(6 \pm 1) \times 10^{-16}$ J respectively ($n = 54$). The increased adhesion toughness is an important feature of the porous OC+DOPA adhesives as more energy is necessary to detach these adhesives and therefore are more resistant to failure. This property makes it suitable for placement in areas of the body that are subject to movement. Commercial adhesives such as cyanoacrylates are unsuitable for placement in such environments because the cured glue is brittle, despite their high adhesive strength [1].

3.3. L-DOPA oxidation

To examine L-DOPA oxidation within the porous OC+DOPA films upon LED irradiation (Fig. 3A), UV–Vis spectra of the films with and without irradiation were recorded (Fig. 3B), after they had been dissolved in 2% v/v acetic acid to record their spectra. Upon irradiation, absorbance within the 300 to 500 nm wavelength range increased. This suggests the accumulation of amine-catecholquinone products (300 – 400 nm) and the formation of catecholquinone coupling derivatives (400 – 500 nm) in the film when irradiated [12,27–29]. These absorbances (300 – 500 nm) are presented together as a broad shoulder (no distinct peaks can be seen) likely due to the absorbance summation of various products [28]. Both films had a peak at 280 nm, which is characteristic of L-DOPA [30], and peaks at 528 nm and 563 nm, which are typical of rose bengal [20]. The oxidation of L-DOPA was also observed visually as the films changed colour from pink to brown.

The advantage of using photo-oxidation is that it avoids the need for premixing or chemical treatment to initiate crosslinking

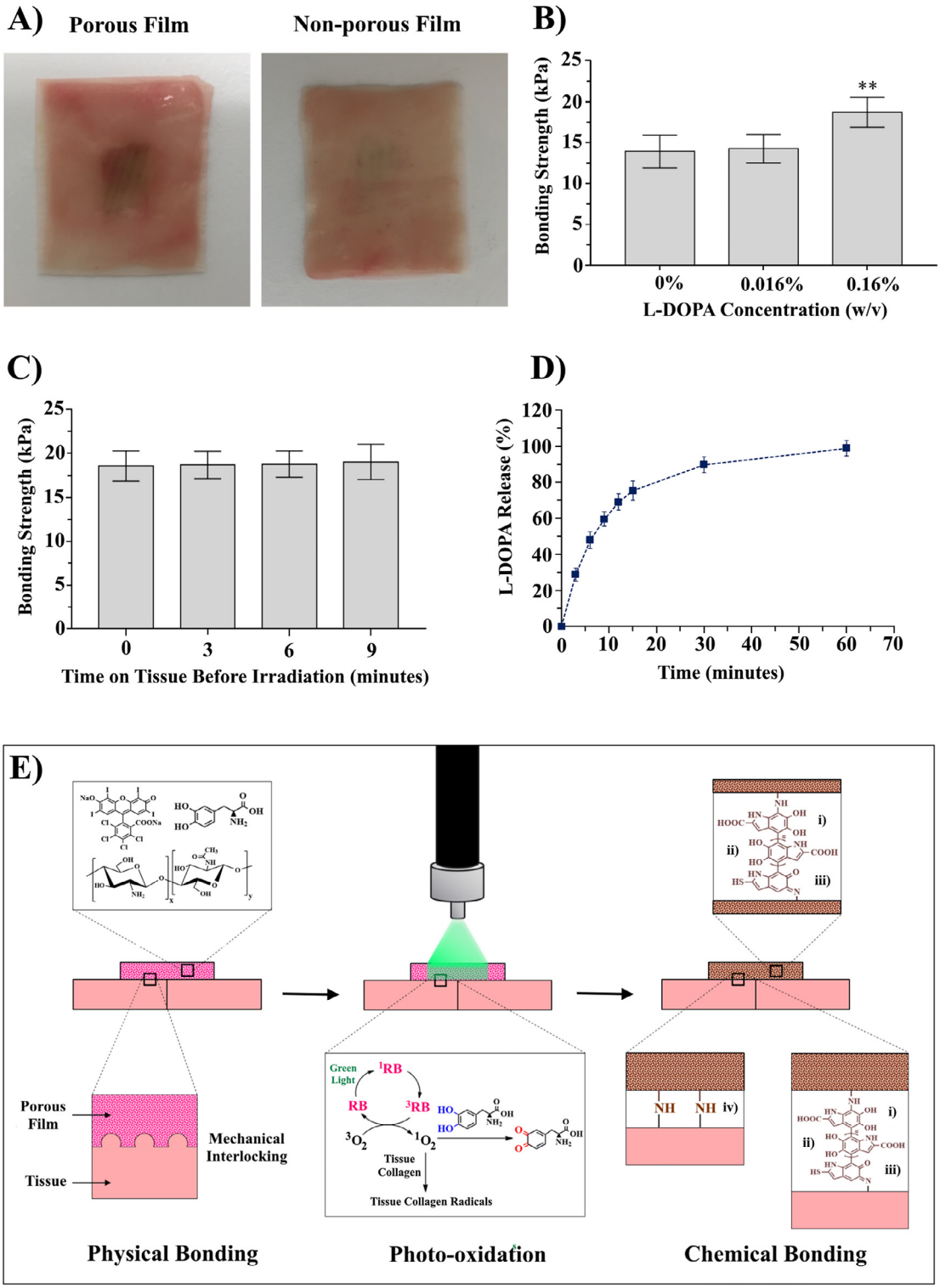

Fig. 4. Analysis of L-DOPA release and mechanisms of tissue adhesion for the porous OC+DOPA film. A) shows typical images of the staining on sheep intestine tissue when porous and non-porous OC+DOPA adhesive films (film size = $1.0 \times 0.6\,cm^2$) were photochemically bonded to the tissue (films were irradiated with green light for ~ 6 min); the dark brown areas are characteristic of oxidised L-DOPA intermediates. Tissue browning was greatest with the porous OC+DOPA film. B) shows the bonding strength of the porous OC+DOPA films with ten times less DOPA (0.016%) and no L-DOPA (0%). The concentration of L-DOPA in this graph refers to the concentration of L-DOPA in the adhesive solution (** $p < 0.005$, one-way ANOVA, Tukey's post-test, $n = 6$). C) shows the effect of release time on the bonding strength of the porous OC+DOPA; the films were left on the tissue for 0, 3, 6 or 9 min before ~ 6 min of irradiation; there was no significant difference between groups ($p > 0.05$, one-way ANOVA, $n = 6$). D) shows the percentage of L-DOPA from the porous OC+DOPA films when left in 5 mL of PBS at room temperature for different time intervals (for each point, $n = 3$). E) shows possible bonding mechanisms for the porous OC+DOPA films on tissue. Without green light exposure, this porous film primarily bonds to tissue through mechanical interlocking. When these films are exposed to a LED green light, the rose bengal dye (RB) absorbs the light and produces singlet oxygen at the tissue interface, which can in turn facilitate the oxidation of L-DOPA and tissue collagen [16,17]. The L-DOPA oxidation products can initiate the crosslinking between tissue collagen and the amino groups of chitosan through i) Michael addition and iii) Schiff base reactions [12,29]. The photo-oxidation can also promote the polymerisation of L-DOPA into oligomers as shown in ii) [12,29,32]. The tissue collagen radicals generated from the photo-oxidation may also initiate the crosslinking of chitosan's amino groups with the tissue surface as shown in iv) [16,17]. (For interpretation of the references to color in this figure legend, the reader is referred to the web version of this article.)

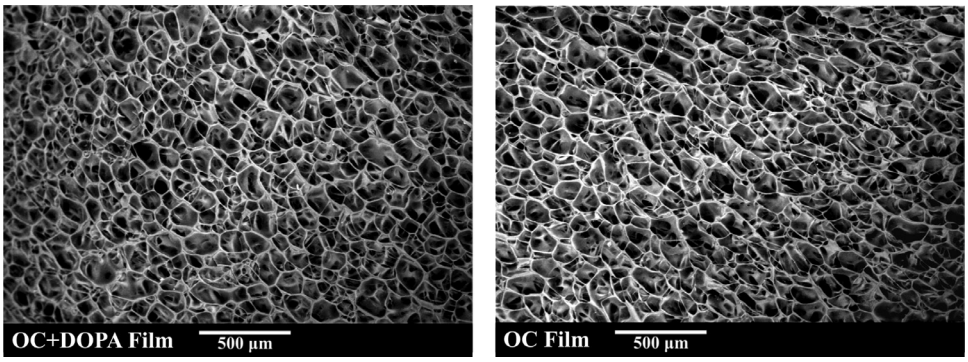

Fig. 5. SEM images showing the surface of a typical porous adhesive film made from the OC+DOPA composition and the OC composition. The pores in both films were interconnected and ~ 110 µm in diameter.

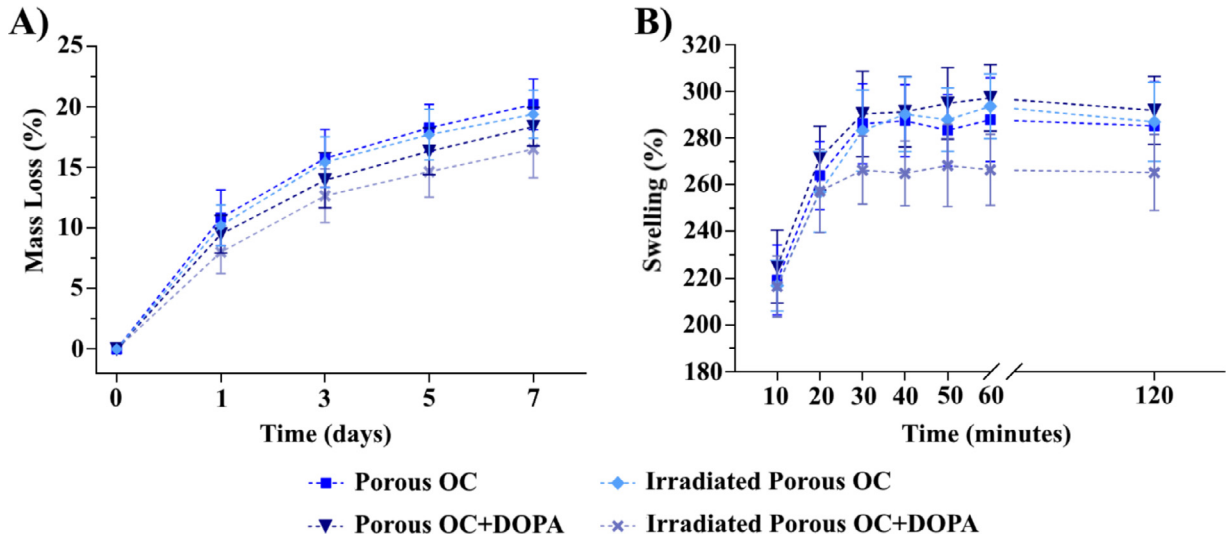

Fig. 6. Percentage mass loss (A) and percentage mass swelling ratio (B) of porous OC+DOPA films with and without irradiation in PBS at 37 °C. Each point represents mean ± standard deviation ($n = 6$). The percentage mass loss of the irradiated porous OC+DOPA films and porous OC films were significantly different at day 5 and day 7 ($p < 0.05$, one-way ANOVA, Tukey's post-test). The irradiated porous OC+DOPA film had lower swelling ratios than the porous OC+DOPA film at each timepoint after 30 min ($p < 0.05$, one-way ANOVA, Tukey's post-test).

reactions. The use of light is easier to apply and will allow the surgeon to control more precisely, when, where and how long the adhesive is crosslinked. Many of the catechol modified adhesives reported in the literature, use oxidising agents such as periodate or ferric ions, which can cause allergic reactions [22,23]. Other reported adhesives have used oxidising enzymes such as tyrosinase but are limited by production issues despite their better biocompatibility [22,23]. Furthermore, the level of reactive oxygen species produced by photoactivated rose bengal for PTB has been confirmed to be biocompatible when tested *in vitro, in vivo* and in a clinical trial [2,3,31].

3.4. L-DOPA release

The amount of L-DOPA released from the films was qualitatively examined to understand why the porous OC+DOPA films had an increased bonding strength; these tests were done under similar conditions as the adhesion tests (*e.g.* room temperature and contact time with tissue = same time in PBS). No oxidation peaks from L-DOPA were observed during these measurements. The amount of L-DOPA released from the porous OC+DOPA films was greater than the non-porous ones after 6 min in PBS. This is expected as the porous films contain more L-DOPA, which was outlined previously in Section 2.11. Therefore, to compare the release of L-DOPA between the non-porous and porous films, the percentage mass ratios were calculated. The percentage mass ratio of L-DOPA in the non-porous OC+DOPA films to the porous OC+DOPA was ~ 77% (mass of L-DOPA in non-porous film: mass of L-DOPA in porous film). The percentage mass ratio of L-DOPA released into PBS from the non-porous OC+DOPA films to the porous OC+DOPA films was ~ 67% (mass of L-DOPA released from non-porous film: mass of L-DOPA released from porous film). These results indicate that the porous OC+L-DOPA films release L-DOPA at a faster rate than the non-porous OC+L-DOPA films. This faster release of L-DOPA from the porous OC+L-DOPA films correlates well with the observations shown in Fig. 4, where the distinctive brown colour due to the oxidation of L-DOPA was more accentuated in tissue repaired with the irradiated porous OC+DOPA films (Fig. 4A) and when these films had 10 times less L-DOPA, the bonding strength decreased (Fig. 4B). The bonding strength of the films also does not decrease as release time increases; when we left the adhesive film on the tissue for 0, 3, 6 or 9 min before the 6 min of irradia-

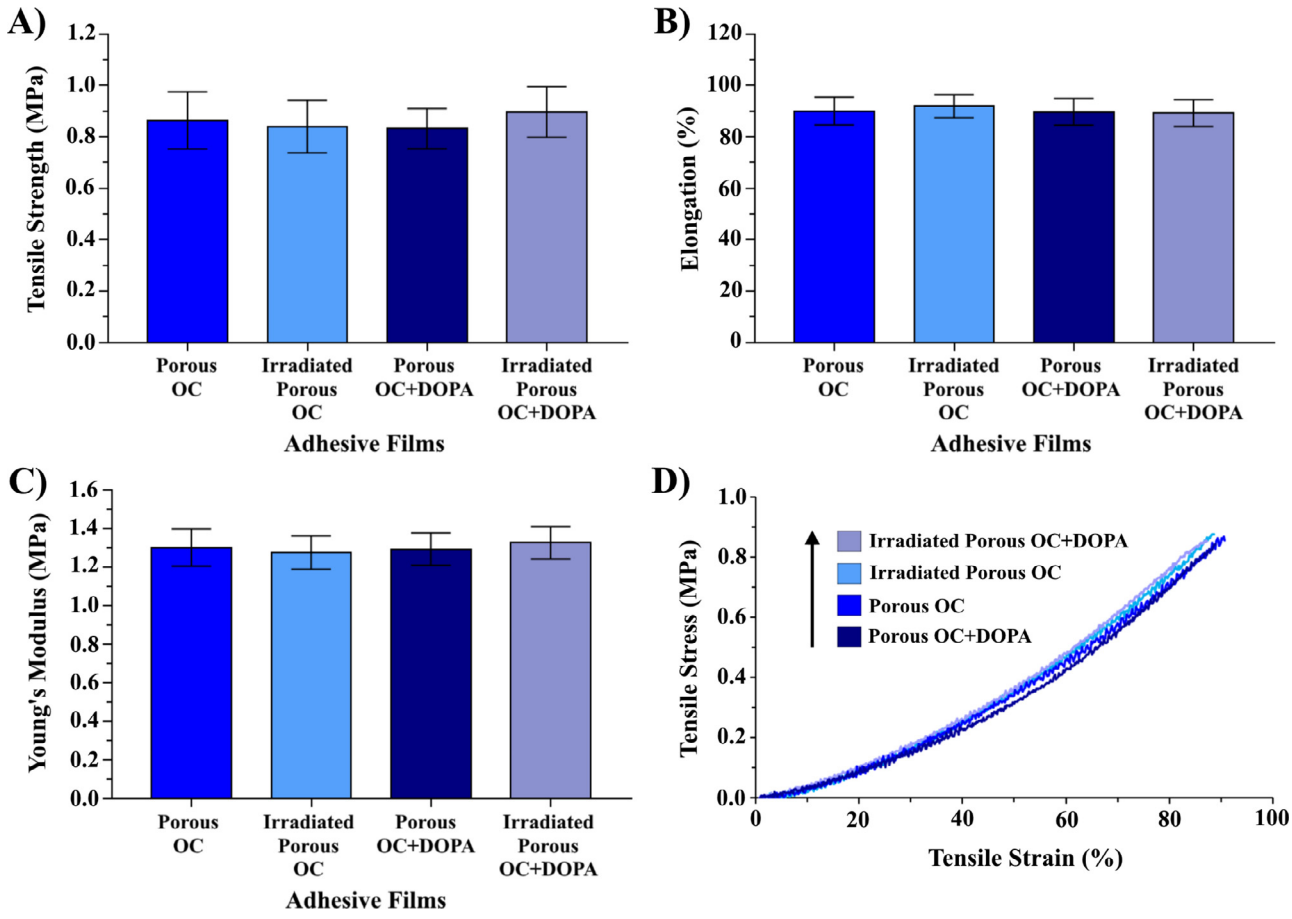

Fig. 7. Tensile strength (A), percentage elongation (B), Young's modulus (C), and representative stress *vs* strain profiles (D) of the irradiated and non-irradiated porous films with or without L-DOPA. The films were tested in the hydrated state to mimic *in vivo* conditions. Data represents mean ± standard deviation ($n = 10$ for each group). There was no significant difference between any of the groups ($p > 0.05$, one-way ANOVA, Tukey's post-test).

tion, the bonding strength for these groups were not significantly different (Fig. 4C). It seems that L-DOPA accumulates at the interface between the film and tissue and most of the L-DOPA may be released during this time; about 50% of L-DOPA is released from the film when left in PBS at room temperature for 6 min (Fig. 4D). Therefore, the high bonding strength of the porous OC+DOPA adhesive may be attributed to the increased amount of crosslinking reactions between the chitosan film and tissue surface due to the presence of more reactive catecholquinones formed at the interface; the oxidised L-DOPA molecules can be thought of like a bridge that covalently links the chitosan with the functional groups on the tissue surface [9]. The transformation of L-DOPA to catecholquinones is initiated by singlet oxygens produced by rose bengal molecules when irradiated with green light [16,17]. The catecholquinones promote crosslinking as they can react with the chitosan amino groups and tissue collagen amino groups through Schiff base and Michael addition reactions [12,18,29]. A summary of possible tissue adhesion mechanisms for this film is presented in Fig. 4E.

3.5. Porous structure

The addition of L-DOPA at 0.16% w/v did not significantly affect the interconnected microporous structure of the films (Fig. 5). The pore diameter of the OC+DOPA and OC porous films were 108 ± 22 µm and 110 ± 24 µm respectively ($p > 0.05$, unpaired *t*-test, $n = 300$). The efficacy of porous chitosan scaffolds as viable supports for facilitating tissue regeneration has been demonstrated in several reports [33]. The pore size can also be made smaller or larger to suit specific cell sizes by adjusting the cooling conditions (temperature and time) before freeze drying [34,35].

3.6. Erosion and swelling

The percentage mass loss of the porous OC+DOPA films after 7 days in PBS at 37 °C was comparable to the porous OC films (day $7 = 18 \pm 2\%$ *vs* $20 \pm 2\%$, $n = 6$, $p > 0.05$, one-way ANOVA, Tukey's post-test). A similar result was also obtained when compared at day 1, 3 and 5. Irradiation did not significantly change the erosion rate of the films ($p > 0.05$, one-way ANOVA, Tukey's post-test), which is in agreement with a previous study that found no significant effect of irradiation on the degradation rate of chitosan films [5]. The irradiated porous OC+DOPA films however, eroded significantly less than the non-irradiated porous OC films at day 5 and day 7 ($p < 0.05$, one-way ANOVA, Tukey's post-test). The erosion profile of these films is shown in Fig. 6A.

The swelling ratios of the porous OC+DOPA films and porous OC films were not significantly different at each timepoint within the 2 h interval of incubation ($p > 0.05$, one-way ANOVA, Tukey's post-test). Irradiation did lower the swelling ratios at each timepoint after 30 min for the porous OC+DOPA films ($p < 0.05$, one-way ANOVA, Tukey's post-test) as shown in Fig. 6B.

The presence of crosslinking products formed in the irradiated porous OC+DOPA films, as seen in Fig. 4C, may contribute to the reduction of its swelling and solubility. The formation of L-DOPAquinone intermediates and the resulting crosslinks formed

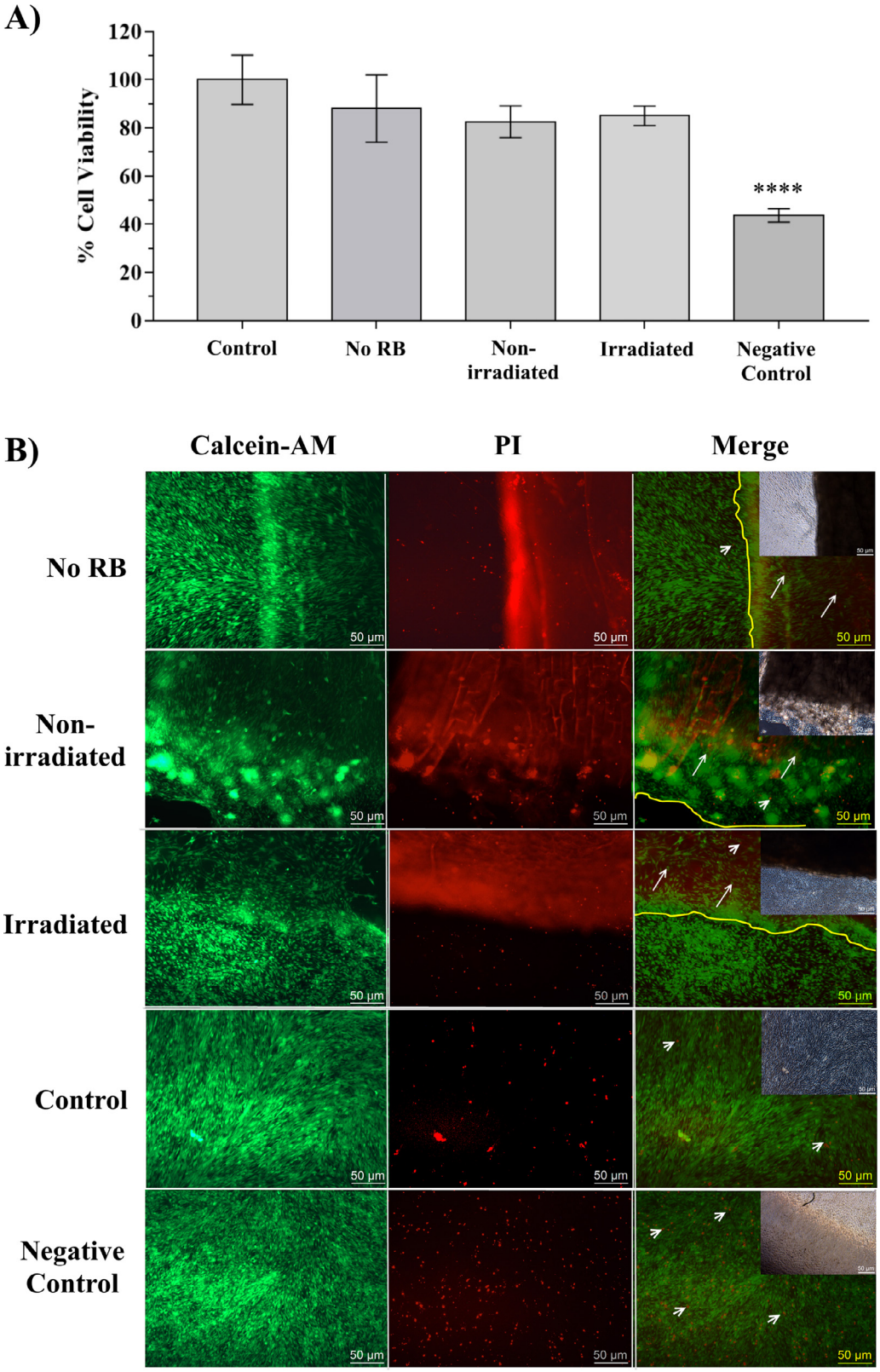

Fig. 8. Assessment of% cell viability (A) and representative live (green)/dead (red) images (B) of cells seeded on OC+DOPA films after 6 days *in vitro*; cells incubated without the films were used as controls and cells treated with 6% ethanol were used as negative controls. Cell viability was quantified based on the reduction of MTT compound by fibroblast cells. Data is displayed as mean ± standard deviation where $n = 4$, in duplicates. P values were determined by one-way ANOVA, Tukey's post-test, where **** signifies $p < 0.0001$. In B) arrows indicate live cells (infiltrating the film) and arrowheads indicate dead cells. Respective brightfield images are also shown as insets. Calcein-AM was used for the green fluorescence and PI as the red fluorescence. Red fluorescence was observed from the films, but this did not affect the qualitative analysis of the cells. Scale bar = 50 µm. (For interpretation of the references to color in this figure legend, the reader is referred to the web version of this article.)

with chitosan in the films have been observed in the UV–Vis spectra shown in Fig. 3B. Rose bengal molecules may initiate the formation of reactive oxygen species, namely singlet oxygen [36], which can easily oxidise the L-DOPA molecules into various L-DOPAquinone intermediates. These molecules can covalently bond with the amino groups of chitosan and polymerise with other catechols to form melanin like conglomerates, which have hydrophobic properties [12,32]. A similar process has been indicated to explain the reduced hydrophilicity of periodate-oxidised L-DOPA-chitosan films [32].

3.7. Mechanical properties

When the porous OC films with or without L-DOPA were LED-irradiated, the mechanical properties (tensile strength, percentage elongation and Young's modulus) did not change significantly ($p > 0.05$, one-way ANOVA, Tukey's post-test). These results suggest that rose bengal does not significantly crosslink the chitosan molecules in the films when irradiated, which is in agreement with previous reports [5,37]. The results also indicate that the concentration of L-DOPA introduced into the films and the self-crosslinking between chitosan and L-DOPA following LED irradiation (Fig. 3) does not meaningfully influence the film's mechanical properties. This may be because the concentration of L-DOPA was low (solution concentration = 0.16% w/v) and that the mechanical tests were performed immediately after the LED irradiation. In another study, periodate oxidised chitosan films with L-DOPA at much higher concentrations (solution concentrations = 5 – 20% w/w) were significantly stiffer than pure chitosan films [32]. The ability of L-DOPA to autooxidise may also affect the adhesive mechanical properties in the medium (weeks) and long-term (months) by limiting their shelf life. More studies are needed to evaluate the mechanical properties and bonding strength of the adhesives after several weeks of storage. It is nonetheless possible to slow down the autooxidation process by storing the adhesives in a vacuum sealed environment.

3.8. Biocompatibility study

The porous OC+DOPA films with and without green light irradiation were compatible with human fibroblasts *in vitro*. The same result was obtained for OC+DOPA films without rose bengal. Cell viability tests revealed no change in metabolic activities in the fibroblasts growing on all the OC+DOPA films and those attached to the dishes (Fig. 8A). The films retained similar level of cell viability compared to that of control cells that were attached directly on the dishes. The films also showed significantly increased cell viability compared to that of the negative control cells ($p < 0.0001$, one-way ANOVA, Tukey's post-test). Cell viability and film penetration was also qualitatively assessed by live/ dead cell staining using Calcein-AM and PI. Live fibroblasts (green) were shown to heavily infiltrate (arrows) into the films irrespective of irradiation, rose bengal and L-DOPA (Fig. 8B). Even though dead cells (red) were present in small amounts in all the groups including the control group, they were much lower compared to that of negative control group (arrowheads); red fluorescence from the films was also observed but this did not affect the qualitative analysis of the cells. Therefore, the concentration of L-DOPA and rose bengal in the adhesive is safe for cells and the crosslinking products in the adhesive formed after irradiation (see Fig. 3) are not cytotoxic. Furthermore, reports have shown that chitosan–catechol porous patches produce no significant inflammatory responses when used *in vivo* [10,38].

4. Conclusion

The adhesive film made in the work through a judicious blend of biocompatible materials including medium weight chitosan, oligomeric chitosan, rose bengal and L-DOPA was fabricated and tested *in vitro*. This film had the following remarkable properties: (1) a higher photochemical tissue bonding strength and adhesion energy than previous non-porous rose bengal-chitosan adhesives, (2) a porous, erodible and elastic structure that is biocompatible with human cells and (3) a simple and scalable manufacturing procedure involving mixing of components, lyophilising and air-drying. These adhesives are suitable for providing strong tissue support without sutures and facilitating tissue repair in surgical procedures, which paves the way for sutureless wound healing.

Acknowledgments

This work was supported by the School of Science and Health, the School of Medicine and the Advanced Materials Characterisation Facility at Western Sydney University, NSW, Australia.

Supplementary materials

Supplementary material associated with this article can be found, in the online version, at doi:10.1016/j.actbio.2019.10.046.

References

[1] A. Lauto, H. Ruprai, J.M. Hook, Adhesives: tissue repair and reconstruction, in: M. Mishra (Ed.), Concise Encyclopedia of Biomedical Polymers and Polymeric Biomaterials, Taylor & Francis, United States, 2017, pp. 1–18.
[2] M.J. Barton, J.W. Morley, M.A. Stoodley, S. Shaikh, D.A. Mahns, A. Lauto, Long term recovery of median nerve repair using laser-activated chitosan adhesive films, J. Biophotonics 8 (2015) 196–207.
[3] A. Lauto, D. Mawad, M. Barton, A. Gupta, S.C. Piller, J. Hook, Photochemical tissue bonding with chitosan adhesive films, Biomed. Eng. Online 9 (2010) 47–57.
[4] N.K. Bhatt, T.R. Khan, C. Mejias, R.C. Paniello, Nerve transection repair using laser-activated chitosan in a rat model, Laryngoscope 127 (2017) E253–E257.
[5] D. Mawad, C. Warren, M. Barton, D. Mahns, J. Morley, B.T.T. Pham, N.T.H. Pham, S. Kueh, A. Lauto, Lysozyme depolymerization of photo-activated chitosan adhesive films, Carbohydr. Polym. 121 (2015) 56–63.
[6] S.J. Frost, D. Mawad, M.J. Higgins, H. Ruprai, R. Kuchel, R.D. Tilley, S. Myers, J.M. Hook, A. Lauto, Gecko-inspired chitosan adhesive for tissue repair, NPG Asia Mater. 8 (2016) e280.
[7] K. Yin, P. Divakar, J. Hong, K.L. Moodie, J.M. Rosen, C.A. Sundback, M.K. Matthew, U.G.K. Wegst, Freeze-cast porous chitosan conduit for peripheral nerve repair, MRS Adv. 3 (2018) 1677–1683.
[8] H. Ruprai, S. Romanazzo, J. Ireland, K. Kilian, D. Mawad, L. George, R. Wuhrer, J. Houang, D. Ta, S. Myers, A. Lauto, Porous chitosan films support stem cells and facilitate sutureless tissue repair, ACS Appl. Mater. Interfaces 11 (2019) 32613–32622.
[9] J. Xu, G.M. Soliman, J. Barralet, M. Cerruti, Mollusk glue inspired mucoadhesives for biomedical applications, Langmuir 28 (2012) 14010–14017.
[10] J.H. Ryu, H.J. Kim, K. Kim, G. Yoon, Y. Wang, G.-S. Choi, H. Lee, J.S. Park, Multipurpose intraperitoneal adhesive patches, Adv. Funct. Mater. 0 (2019) 1900495.
[11] J.H. Ryu, Y. Lee, W.H. Kong, T.G. Kim, T.G. Park, H. Lee, Catechol-functionalized chitosan/pluronic hydrogels for tissue adhesives and hemostatic materials, Biomacromolecules 12 (2011) 2653–2659.
[12] K. Yamada, T. Chen, G. Kumar, O. Vesnovsky, L.D.T. Topoleski, G.F. Payne, Chitosan based water-resistant adhesive. Analogy to mussel glue, Biomacromolecules 1 (2000) 252–258.
[13] D. Lu, H. Wang, X. Wang, Y. Li, H. Guo, S. Sun, X. Zhao, Z. Yang, Z. Lei, Biomimetic chitosan-graft-polypeptides for improved adhesion in tissue and metal, Carbohydr. Polym. 215 (2019) 20–28.
[14] J.H. Kim, J.I. Lim, H.-K. Park, Porous chitosan-based adhesive patch filled with poly(l-3,4-dihydroxyphenylalanine) as a transdermal drug-delivery system, J. Porous Mater. 20 (2013) 177–182.
[15] X. Peng, Y. Peng, B. Han, W. Liu, F. Zhang, R.J. Linhardt, IO4–stimulated crosslinking of catechol-conjugated hydroxyethyl chitosan as a tissue adhesive, J. Biomed. Mater. Res. B 107 (2019) 582–593.
[16] E.I. Alarcon, H. Poblete, H. Roh, J.-F. Couture, J. Comer, I.E. Kochevar, Rose bengal binding to collagen and tissue photobonding, ACS Omega 2 (2017) 6646–6657.
[17] R.W. Redmond, I.E. Kochevar, Medical applications of rose bengal- and riboflavin-photosensitized protein crosslinking, Photochem. Photobiol. 95 (2019) 1097–1115.
[18] J. Yang, M.A. Cohen Stuart, M. Kamperman, Jack of all trades: versatile catechol crosslinking mechanisms, Chem. Soc. Rev. 43 (2014) 8271–8298.

[19] T. Sato, T. Aoyagi, M. Ebara, R. Auzély-Velty, Catechol-modified hyaluronic acid: in situ-forming hydrogels by auto-oxidation of catechol or photo-oxidation using visible light, Polym. Bull. 74 (2017) 4069–4085.
[20] A. Lauto, M. Stoodley, M. Barton, J.W. Morley, D.A. Mahns, L. Longo, D. Mawad, Fabrication and application of rose bengal-chitosan films in laser tissue repair, J. Vis. Exp. 68 (2012) e4158.
[21] S.J. Frost, D. Mawad, R. Wuhrer, S. Myers, A. Lauto, Semitransparent bandages based on chitosan and extracellular matrix for photochemical tissue bonding, Biomed. Eng. Online 17 (2018) 1–14.
[22] V. Bhagat, M.L. Becker, Degradable adhesives for surgery and tissue engineering, Biomacromolecules 18 (2017) 3009–3039.
[23] M. Rahimnejad, W. Zhong, Mussel-inspired hydrogel tissue adhesives for wound closure, RSC Adv. 7 (2017) 47380–47396.
[24] D. Mawad, C. Mansfield, A. Lauto, F. Perbellini, G.W. Nelson, J. Tonkin, S.O. Bello, D.J. Carrad, A.P. Micolich, M.M. Mahat, J. Furman, D. Payne, A.R. Lyon, J.J. Gooding, S.E. Harding, C.M. Terracciano, M.M. Stevens, A conducting polymer with enhanced electronic stability applied in cardiac models, Sci. Adv. 2 (2016) e1601007.
[25] M. Barton, J.W. Morley, M.A. Stoodley, K.S. Ng, S.C. Piller, H. Duong, D. Mawad, D.A. Mahns, A. Lauto, Laser-activated adhesive films for sutureless median nerve anastomosis, J. Biophotonics 6 (2013) 938–949.
[26] S. Rawson, S. Cartmell, J. Wong, Suture techniques for tendon repair; a comparative review, Muscles Ligaments Tendons J 3 (2013) 220–228.
[27] B.P. Lee, J.L. Dalsin, P.B. Messersmith, Synthesis and gelation of dopa-modified poly(ethylene glycol) hydrogels, Biomacromolecules 3 (2002) 1038–1047.
[28] K. Kim, J.H. Ryu, D.Y. Lee, H. Lee, Bio-inspired catechol conjugation converts water-insoluble chitosan into a highly water-soluble, adhesive chitosan derivative for hydrogels and LbL assembly, Biomater. Sci. 1 (2013) 783–790.
[29] X. Zhang, P. Hassanzadeh, T. Miyake, J. Jin, M. Rolandi, Squid beak inspired water processable chitosan composites with tunable mechanical properties, J. Mater. Chem. B 4 (2016) 2273–2279.
[30] D.G. Graham, P.W. Jeffs, The role of 2,4,5-trihydroxyphenylalanine in melanin biosynthesis*, J. Biol. Chem. 252 (1977) 5729–5734.
[31] S. Tsao, M. Yao, H. Tsao, F.P. Henry, Y. Zhao, J.J. Kochevar, R.W. Redmond, I.E. Kochevar, Light-activated tissue bonding for excisional wound closure: a split-lesion clinical trial, Br. J. Dermatol. 166 (2012) 555–563.
[32] D.X. Oh, D.S. Hwang, A biomimetic chitosan composite with improved mechanical properties in wet conditions, Biotechnol. Prog. 29 (2013) 505–512.
[33] J.C.V. Ribeiro, R.S. Vieira, I.M. Melo, V.M.A. Araújo, V. Lima, Versatility of chitosan-based biomaterials and their use as scaffolds for tissue regeneration, Sci. World J. 2017 (2017) 8639898 -8639898.
[34] S.-J. Cai, C.-W. Li, D. Weihs, G.-J. Wang, Control of cell proliferation by a porous chitosan scaffold with multiple releasing capabilities, Sci. Technol. Adv. Mater. 18 (2017) 987–996.
[35] S.V. Madihally, H.W. Matthew, Porous chitosan scaffolds for tissue engineering, Biomaterials 20 (1999) 1133–1142.
[36] P.C. Lee, M.A. Rodgers, Laser flash photokinetic studies of rose bengal sensitized photodynamic interactions of nucleotides and DNA, Photochem. Photobiol. 45 (1987) 79–86.
[37] M.J. Barton, J.W. Morley, D.A. Mahns, D. Mawad, R. Wuhrer, D. Fania, S.J. Frost, C. Loebbe, A. Lauto, Tissue repair strength using chitosan adhesives with different physical-chemical characteristics, J. Biophotonics 7 (2014) 948–955.
[38] J.M. Lee, J.H. Ryu, E.A. Kim, S. Jo, B.S. Kim, H. Lee, G.I. Im, Adhesive barrier/directional controlled release for cartilage repair by endogenous progenitor cell recruitment, Biomaterials 39 (2015) 173–181.